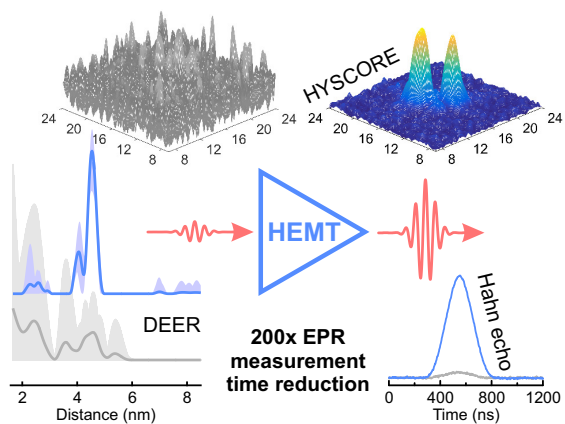# Graphical Abstract

A sensitivity leap for X-band EPR using a probehead with a cryogenic preamplifier

Mantas Šimėnas,James O'Sullivan,Christoph W. Zollitsch,Oscar Kennedy,Maryam Seif-Eddine,Irina Ritsch,Miriam Hülsmann,Mian Qi,Adelheid Godt,Maxie M. Roessler,Gunnar Jeschke,John J.L. Morton

Highlights

A sensitivity leap for X-band EPR using a probehead with a cryogenic preamplifier

Mantas Šimėnas,James O'Sullivan,Christoph W. Zollitsch,Oscar Kennedy,Maryam Seif-Eddine,Irina Ritsch,Miriam Hülsmann,Mian Qi,Adelheid Godt,Maxie M. Roessler,Gunnar Jeschke,John J.L. Morton

- We equipped an X-band EPR probehead with an ultra low-noise cryogenic microwave preamplifier.

- Our setup shortens the measurement time by about 50× at low temperature.

- At the expense of excitation bandwidth, above 200× reduction in the measurement time is obtained.

- The probehead performance is demonstrated using hyperfine and dipolar spectroscopy experiments.

A sensitivity leap for X-band EPR using a probehead with a cryogenic preamplifier

Mantas Šimėnas[a,*], James O'Sullivan[a], Christoph W. Zollitsch[a], Oscar Kennedy[a], Maryam Seif-Eddine[b], Irina Ritsch[c], Miriam Hülsmann[d], Mian Qi[d], Adelheid Godt[d], Maxie M. Roessler[b], Gunnar Jeschke[c] and John J.L. Morton[a,e,*]

[a]*London Centre for Nanotechnology, University College London, London WC1H 0AH, UK*

[b]*Department of Chemistry, Imperial College London, Molecular Sciences Research Hub, London W12 0BZ, UK*

[c]*ETH Zürich, Department of Physical Chemistry, Vladimir-Prelog-Weg 2, 8093 Zürich, Switzerland*

[d]*Faculty of Chemistry and Center for Molecular Materials (CM2), Bielefeld University, Universitätsstraße 25, Bielefeld 33615, Germany*

[e]*Department of Electronic & Electrical Engineering, UCL, London WC1E 7JE, UK*

ARTICLE INFO

ABSTRACT

Inspired by the considerable success of cryogenically cooled NMR cryoprobes, we present an upgraded X-band EPR probehead, equipped with a cryogenic low-noise preamplifier. Our setup suppresses source noise, can handle the high microwave powers typical in X-band pulsed EPR, and is compatible with the convenient resonator coupling and sample access found on commercially available spectrometers. Our approach allows standard pulsed and continuous-wave EPR experiments to be performed at X-band frequency with significantly increased sensitivity compared to the unmodified setup. The probehead demonstrates a voltage signal-to-noise ratio (SNR) enhancement by a factor close to 8× at a temperature of 6 K, and remains close to 2× at room temperature. By further suppressing room-temperature noise at the expense of reduced microwave power (and thus minimum π-pulse length), the factor of SNR improvement approaches 15 at 6 K, corresponding to an impressive 200-fold reduction in EPR measurement time. We reveal the full potential of this probehead by demonstrating such SNR improvements using a suite of typical hyperfine and dipolar spectroscopy experiments on exemplary samples.

1. Introduction

Over the last few decades, cryogenically cooled cryoprobes have become a state-of-the-art tool in NMR spectroscopy resulting in a substantial boost in sensitivity [1–4]. In these probeheads, the NMR coil is cooled down together with a low-noise preamplifier, while a sample can be maintained at room temperature (for example, in the liquid state). Cryogenic cooling provides a significant reduction of thermal noise power, which is proportional to temperature. Ideally, the cold preamplifier amplifies the signal above the room-temperature noise level making it invulnerable to noise introduced between the cryoprobe and the detector. Given a sufficiently low noise temperature of the preamplifier, this provides a significant increase in the signal-to-noise ratio (SNR) [4].

Despite this widespread success in NMR, cryogenic preamplifiers are still rarely used in EPR spectroscopy, even though developments in high electron mobility transistor (HEMT) technology provide microwave amplifiers with gain up to 36 dB and noise temperature lower than 4 K [5]. Several EPR studies reported cryogenic cooling of the amplifiers in the microwave bridge, which resulted in a moderate improvement of sensitivity [6–8]. The SNR increase in such cases originates from the reduction of the amplifier noise temperature on cooling. However, in addition to the require-

ment of an impractical separate cooling circuit, these setups still suffer from thermal noise introduced by the microwave components situated at room temperature.

An EPR probehead with a microwave preamplifier was reported by Rinard *et al.* [9] for a homebuilt pulsed S-band spectrometer. The probehead contained a circulator for routing of microwave signals and a power limiter for protection of the preamplifier. The setup demonstrated a significant voltage SNR improvement of about 8 at room temperature, which occurred mainly due to compensation of high microwave losses in the EPR bridge. However, a circulator alone within the probehead does little to suppress room-temperature noise coming down the input line preventing optimal SNR improvement when operating at cryogenic temperatures. Furthermore, the use of typical ferrite circulators in the vicinity of the sample can be challenging, due to the applied magnetic field.

Cryogenically cooled low-noise HEMT preamplifiers have become commonly used in studies of superconducting microresonators in the context of qubits [10, 11], and this has helped stimulate the use of low-noise preamplifiers in microresonator-based EPR to significantly advance the sensitivity limits of pulsed EPR [12–14]. In low-power continuous-wave (CW) EPR measurements using a planar 14 GHz copper microresonator, the input noise was suppressed by a 10 dB attenuator placed on the probehead containing a low-noise preamplifier, which resulted in a 2.5× reduction in noise amplitude on cooling from 270 to 17 K [15]. A Q-band copper microresonator and cryogenic preamplifier

were employed to achieve a sensitivity of 7000 spins/$\sqrt{\text{Hz}}$ at 10 K [16]. Using superconducting microresonators and a quantum-limited amplifier before the HEMT, an impressive sensitivity of 65 spins/$\sqrt{\text{Hz}}$ was demonstrated at milliKelvin temperatures [17].

While these works have pushed the boundaries on spin sensitivity, the broader applicability of these approaches in conventional pulsed EPR spectroscopy is still limited due to the operation at low microwave powers, the requirement of non-standard resonators and sample handling, and a lack of compatibility with commercially available spectrometers. Furthermore, in many cases it is not spin number, but spin concentration sensitivity which is most desirable, favouring more conventional three-dimensional resonators, and their simple sample access, over planar microresonators.

In this communication, we present a cryogenically cooled X-band EPR probehead which is equipped with a low-noise HEMT preamplifier and meets all the requirements for standard pulsed and CW EPR experiments. Our demonstration is based on a modified Bruker EPR probehead fitted with a standard dielectric resonator, retaining its straightforward sample access and coupling. Our approach can be readily used with other resonators and other probehead designs. By maintaining the ability to work with high microwave powers, our probehead permits the standard suite of EPR experiments to be performed, which we illustrate here through double electron-electron resonance (DEER) and hyperfine sublevel correlation spectroscopy (HYSCORE) on exemplary samples. In all cases, we see a substantial increase in the SNR across a broad range of temperatures due to the use of a low-noise HEMT preamplifier, suppression of source noise and the reduction of losses between the sample and the first preamplifier.

2. Probehead design

Our setup is based on a modified Bruker ER 4118SPT probehead equipped with a Bruker X-band ER 4118X-MD5W microwave resonator and connected to a Bruker ELEXSYS E580 EPR spectrometer. It is designed to handle the high microwave powers from a 1 kW traveling-wave tube (TWT) amplifier commonly used in X-band EPR, as well as to retain conventional 'top-loading' sample access and resonator coupling capabilities found on these probeheads. The design, schematically represented in Fig. 1, consists of a semirigid input line, which is used to send high power pulses to the resonator via a coupled port of a (e.g.) 6 dB or 30 dB directional coupler (Pasternack PE2CP series) situated next to the resonator. The attenuation on this coupled port suppresses thermal noise from room temperature (improving SNR) but also limits the maximum power (and hence bandwidth) of the applied microwave pulses. Reflected signals and spin echoes coming from the resonator are directed by the same directional coupler to a Narda LIM-301 limiter (500 W peak power, 130 mW flat leakage, < 200 ns recovery time and 0.1% duty cycle), which is used to protect the subsequent microwave components in the circuit (in particular

the HEMT). A fast non-reflective switch (Analog Devices HMC547ALP3E, < 20 ns switching time, 40 dB isolation) is used for further protection: during high power microwave pulses, the switch diverts the reflected pulses to a 50 Ω load. The switch is controlled using a signal from the "Receiver Protection 2" channel in the Bruker console, converted to the required voltage level using a homebuilt board. The spin signal is amplified by a Low Noise Factory LNF-LNC6_20C cryogenic HEMT preamplifier (34 dB gain and noise temperature of 2.5 K at 4 K and 70 K at room temperature). The HEMT is thermalized via a copper arm extending below the resonator. The amplified signal leaves the probehead via a second output microwave line.
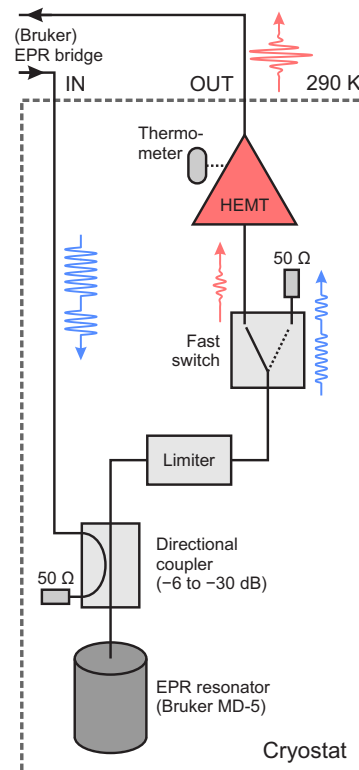

Figure 1: Schematic of the microwave circuit within our modified probehead with the low-noise cryogenic preamplifier. Microwave excitation signals (blue) that are reflected from the resonator are diverted to a 50 Ω load, while spin echo signals (red) are amplified by the HEMT, benefiting from its low noise temperature. DC lines for the HEMT, temperature sensor and fast microwave switch are not shown for clarity. In practice, all components are closely integrated to facilitate a low HEMT temperature.

In contrast to the conventional reflection setup, the modified probehead has two microwave ports for input and output signals. In principle, both lines can be joined on top of the cryostat using a circulator and then connected to the bridge, however, this can introduce additional interferences. A better solution is therefore to operate in transmission mode, either by using the secondary input port available on some EPR bridges, or by making a simple modification to the bridge to bypass the internal circulator.

3. Results and Discussion

3.1. SNR Improvement at Different Temperatures

We investigated the performance of our probehead at different temperatures by measuring the Hahn echo of a standard coal sample and comparing it to the unmodified setup (see Supplementary material for experimental details). The measurements were performed using a 6 dB directional coupler allowing us to use π-pulses of 40 ns duration. We compensated the pulse power to account for the directional coupler in our modified setup so that the pulse bandwidth was the same for both experiments. The echoes, normalized to the noise level and obtained at 6 and 290 K, are presented in Figs. 2a and S1 (Supplementary material), respectively. A sensitivity improvement can be observed at both temperatures with a corresponding increase of voltage SNR by a factor of 9.6 ± 0.6 and 3.2 ± 0.2. This translates to a significant reduction of measurement time by a factor of about 90 and 10, respectively. A substantial SNR improvement at room temperature was also obtained using the low-noise preamplifiers in CW mode [8, 18, 19]. The temperature dependence of the SNR improvement is presented in Fig. 2c revealing its gradual decrease with increasing temperature.

The expected voltage SNR improvement can be estimated by assuming that the main noise mechanism in our system is thermal noise with a noise level in voltage given by $N = A\sqrt{T}$, where A is constant for both measurement setups. We also assume that the noise level in a standard setup corresponds to 290 K, since the detection circuit and the microwave amplifier are situated at room temperature. In this case, the SNR for our unmodified setup without any additional components is

$$\mathrm{SNR}_0 = \frac{1}{A\sqrt{290\,[\mathrm{K}] + T_B}} \frac{S}{L_{\mathrm{RB}}}, \tag{1}$$

where the spin signal S emitted from the resonator (R) is attenuated by a factor L_{RB} until it is amplified in the microwave bridge (B), and T_B denotes the noise temperature of the microwave amplifier. In contrast, we assume that the noise level in the HEMT setup is determined by the sample temperature T_S, as the preamplifier with a 34 dB gain should amplify the signal significantly above the room-temperature noise level. The temperatures of the sample and additional microwave components were equal during the experiments (see Supplementary material for details). Here, we also ignore the noise temperature of the HEMT, as it is much smaller than the sample temperature in the investigated temperature range. However, in this case the spin signal from the resonator (R) is attenuated by a factor L_{RH} due to additional components in front of the HEMT (H). The SNR for the modified setup can then be expressed as

$$\mathrm{SNR}_H = \frac{1}{A\sqrt{T_S}} \frac{S}{L_{\mathrm{RH}}}, \tag{2}$$

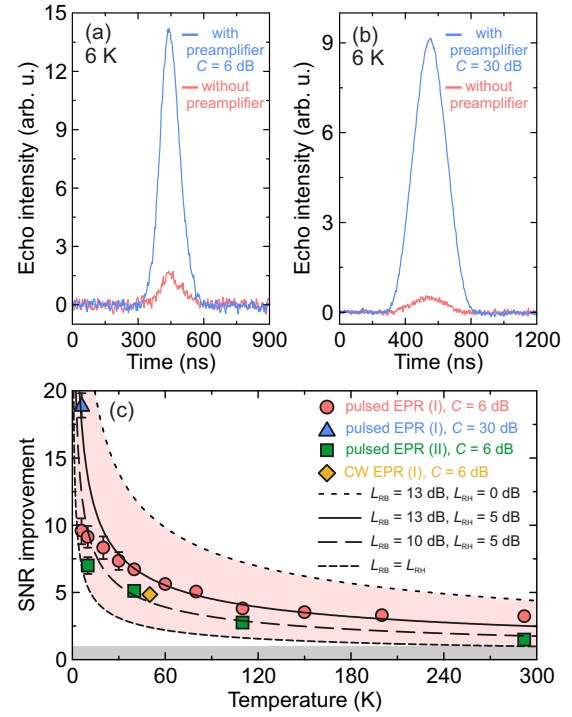such that the estimated voltage SNR improvement can be

Figure 2: Hahn echoes of the coal sample obtained at 6 K using the HEMT probehead and the standard unmodified setups. Measurements with the preamplifier were performed using a directional coupler of (a) 6 dB and (b) 30 dB coupling. Signals are normalized to the noise level. Experimental parameters: (a) $\tau = 4$ µs, 10 averages, $t_\pi = 40$ ns and (b) $\tau = 4.5$ µs, 50 averages, $t_\pi = 200$ ns. (c) Temperature dependence of the SNR improvement measured using pulsed and CW EPR. For pulsed experiments, two different Bruker E580 spectrometers (I and II) were used. Pink area indicates the region of theoretical SNR enhancement bounded by the dashed curves representing the cases of an ideal probehead ($L_{\mathrm{RH}} = 0$ dB) and $L_{\mathrm{RB}} = L_{\mathrm{RH}}$ (see text for definition of $L_{\mathrm{RH}} = 0$ and $L_{\mathrm{RB}} = 0$). The gray region marks SNR improvement less than one. If not indicated, the error bar is smaller than the data point.

obtained by taking the ratio:

$$\frac{\mathrm{SNR}_H}{\mathrm{SNR}_0} = \sqrt{\frac{290\,[\mathrm{K}]}{T_S}} \frac{L_{\mathrm{RB}}}{L_{\mathrm{RH}}}, \tag{3}$$

where the amplifier noise temperature T_B has been incorporated into the bridge noise figure L_{RB} (see Supplementary material for details). Note that the obtained equation can be also obtained from the Friis equation [8] under the simplifications listed above.

Through a benchtop measurement we found the power attenuation from the resonator to the HEMT to be about 5 dB at room temperature (lower losses are expected at low temperature), which translates to $L_{\mathrm{RH}} = 1.8$. Taking this value, the fit of Eq. 3 to the experimental data provides $L_{\mathrm{RB}} = 4.5$ (Fig. 2c), which corresponds to 13 dB power attenuation. Using these values and above assumptions, we simulated the signal and noise propagation at different stages of both setups as demonstrated in Fig. S2.

We performed the same type of measurements at several selected temperatures using another Bruker EPR spectrometer to rule out that the first spectrometer was performing anomalously badly, enhancing our reported gains. The SNR improvement from the second spectrometer is a factor of 1.3-1.4 smaller in the whole investigated temperature range resulting in L_{RB} of about 10 dB for the second spectrometer (see Fig. 2c). This indicates that the noise figure of the first spectrometer is about 3 dB higher (see Supplementary material for details). However, as it is our main spectrometer, it was used to perform the subsequent experiments.

By setting $L_{RH} = 1$ (0 dB) and $L_{RB} = 4.5$ (13 dB), we obtain the ideal probehead case, which bounds the theoretical upper limit of SNR improvement using our setup (see Fig. 2c). As the lower bound, we have chosen $L_{RB} = L_{RH}$ case, which corresponds to the same detection circuit in the microwave bridge and on the probehead. In this case, the SNR improvement occurs solely due to the reduction of thermal noise of the microwave components.

Fig. 2c shows that at temperatures below about 30 K, the measured SNR improvement is smaller than predicted by the arguments above. This can be attributed to an additional noise source, most likely room-temperature noise from the TWT (see Supplementary material) coming down the input line, which is only partially attenuated by the 6 dB directional coupler before reaching the resonator. To fully suppress such noise, we used a 30 dB directional coupler, which also necessitated much longer π-pulses of 200 ns duration. The Hahn echo obtained at 6 K using the HEMT probehead with a 30 dB coupler is presented in Fig. 2b together with the same measurement performed using the unmodified setup. A striking increase in SNR by a factor of 18.8 ± 0.7 (350-fold decrease in measurement time) is observed, in excellent agreement with the theoretical prediction. We did not perform this experiment on our second less lossy spectrometer, but here we also expect the SNR improvement to be a factor of about 1.3 lower. For the subsequent experiments described below, we used a 6 dB directional coupler.

We also measured the echo-detected field sweep (EDFS) spectra of the coal sample at 6 and 290 K by integrating the Hahn echo. The obtained spectra are presented in Fig. S3 revealing the same factors of SNR improvement as determined from the echo experiments. More importantly, the spectra measured with our probehead are in an excellent agreement with the experiments performed using the standard setup. This demonstrates that the introduced modifications do not distort the lineshape.

The design of our setup is also compatible with CW EPR, which we confirmed through measurements on Cu(II) centers in $[(CH_3)_2NH_2][Zn(HCOO)_3]$ metal-organic framework [20]. The measured spectra are presented in Fig. S4 revealing an SNR enhancement by a factor of 4.9 ± 0.4 at 50 K, which is slightly lower than obtained from the pulsed EPR (Fig. 2c). As discussed by Rinard *et al.* [9], a lower value of SNR improvement is indeed expected for the CW mode due to additional noise introduced by the microwave source, which is present during the signal acquisition. The compat-

ibility of our setup with the CW measurements eliminates the need to change or modify the probehead when switching between different modes of the experiment. However, care should be taken during the measurements at higher power, as this HEMT is specified only up to 1 mW input CW power.

3.2. HYSCORE

To further illustrate the potential of our probehead, we performed HYSCORE experiments at 10 K on a *Bos Taurus* respiratory complex I sample, which was previously investigated in Ref. [21] (see Supplementary material for experimental details). The ^{1}H HYSCORE spectra obtained in 1 hour of signal averaging with and without the preamplifier are presented in Fig. 3. The measurements were performed using $\tau = 262$ ns to suppress the matrix proton signal. The spectrum obtained with the HEMT probehead shows strong ^{1}H ridges peaked at (14.1, 16.4) and (16.4, 14.1) MHz (Fig. 3a), while these signals are barely resolved using the standard setup (Fig. 3b). The increase in the SNR is better revealed in the 3D plots presented in Figs. 3c and d. The corresponding HYSCORE spectra of non-suppressed matrix protons ($\tau = 296$ ns) are presented Fig. S5, where the proton peak has much stronger intensity and thus it is also rather well visible using the standard probehead.
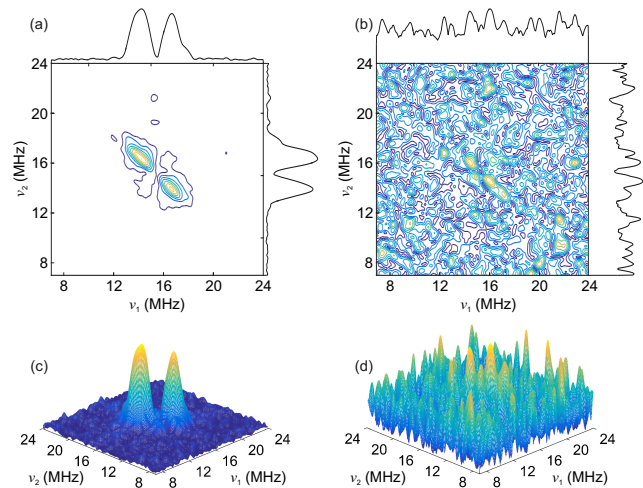

Figure 3: Contour plots with the skyline projections of the ^{1}H HYSCORE spectra of *Bos Taurus* complex I measured using (a) HEMT and (b) standard setups. The corresponding 3D plots are presented in (c) and (d). Spectra were obtained at 10 K and 357.7 mT using $\tau = 262$, $t_{\pi/2} = 16$, $t_{\pi} = 28$ ns and an acquisition time of 1 hour.

For both values of τ, we estimated the SNR enhancement to be about 9, which is in a perfect agreement with the Hahn echo experiments of the coal sample obtained at the same temperature. Note that the SNR improvement would be lower by about a factor of 1.3 using our less lossy spectrometer. Our HYSCORE measurements demonstrate that our probehead is fully compatible with more advanced EPR experiments and could be used to significantly extend the capabilities of the hyperfine spectroscopy at X-band.

The SNR improvement is crucial for metalloproteins, especially those that can only be obtained in small concentrations such as membrane proteins (as is the case here), enzymes contained in extremophiles and in eukaryotic cells that cannot be overexpressed. In addition to the low concentration issue, the EPR characterization of metalloenzymes often involves isotope labelling [22–24] and mutations of amino acids [21, 25], which typically lead to a considerable decrease in the yield of an enzyme further complicating experiments at X-band. In addition, overlapping HYSCORE signals require spectral subtraction [26] or relaxation filters [21, 27]. More sensitive hyperfine measurements at Q-band cannot substitute those at X-band as frequently both bands complement each other [24, 25, 28, 29]. The SMART-HYSCORE sequence has been proposed to avoid blind spots and enable correlation of frequencies stemming from different nuclei[21, 30], however, it usually necessitates long acquisition times on proteins (e.g. 72 h as reported in Ref. [21]). The substantial SNR improvement seen with our probehead could make such experiments much more widely applicable.

3.3. DEER

We used the nitroxide (40 µM, expected mean distance 4.2 nm) and Cu(II) (200 µM, expected mean distance 4.5 nm) rulers depicted in Fig. S6a and b to demonstrate the SNR improvement for dipolar spectroscopy at X-band (see Supplementary material for experimental details). The DEER experiments were, respectively, performed at 50 and 10 K – typical measurement temperatures for these paramagnetic centers. Acquisition of the data took 3 and 30 minutes for the nitroxide and Cu(II) ruler, respectively. The positions of the pump and observer pulses are indicated in the EDFS spectra (Fig. S7), which also show an excellent agreement of the lineshapes measured using both setups. The primary DEER data $V(t)/V(0)$ of both compounds obtained with and without the preamplifier are presented in Fig. S8, while the corresponding background corrected form factors $F(t)/F(0)$ are shown in Fig. 4a and b. A modulation can be readily observed for both samples measured with the HEMT, while the SNR is significantly worse for traces obtained using the standard setup.

We interpreted the DEER data of both rulers in terms of distance distributions using model-free Tikhonov regularization [31]. The obtained distributions for the nitroxide compound are presented in Fig. 4c. A peak is found in the expected distance range for both setups, though it is much broader with the standard probehead compared to the HEMT setup (FWHM of 0.59 vs. 0.25 nm). Such artificial broadening is expected because poor SNR necessitates a larger regularization parameter, which in turn causes oversmoothing of the genuinely narrow distance distribution. The validation performed using DeerAnalysis2019 [32] shows that the distance distribution is highly uncertain over large distance intervals without the preamplifier. In contrast, the uncertainty is strongly reduced using the HEMT probehead. The SNR improvement was estimated from the fit residuals
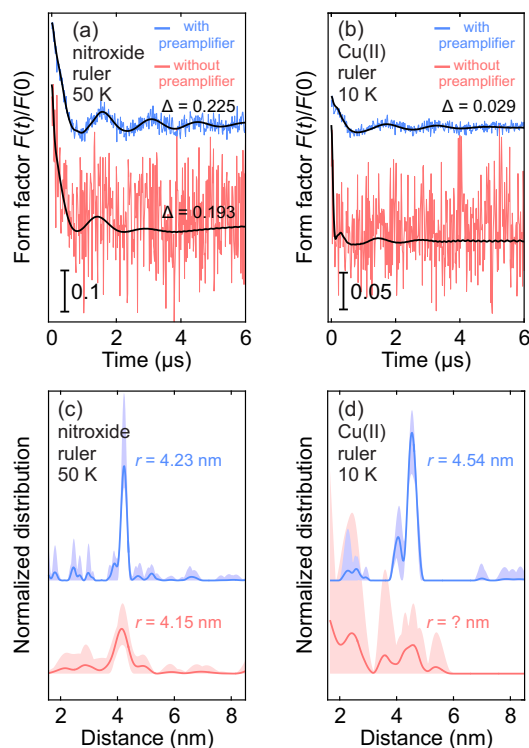

Figure 4: Normalized form factors after the background correction of (a) nitroxide and (b) Cu(II) rulers measured with and without the preamplifier. (c,d) The corresponding distance distributions obtained by Tikhonov regularization. The black curves in (a) and (b) are the form factor fits; Δ denotes the modulation depth. The shaded regions in (c) and (d) denote the uncertainty estimate of the distance distributions obtained from the validation. The indicated distances correspond to the maxima of the distributions. Spectra were obtained at (a) 50 K and (b) 10 K with pulse lengths of 32 ns for observer pulses and of 40 ns for the pump pulse. Acquisition times: (a) 5 min and (b) 30 min.

of the time domain data resulting in a factor of 6.7, which is in a good agreement with the Hahn echo measurements of the coal sample at this temperature (see Fig. 2c).

In the case of Cu(II)-Cu(II) distance measurements using the Cu(II) ruler, the DEER data acquired with the conventional X-band setup show the expected oscillations (see Fig. S8b), but the SNR is very poor leading to unstable analysis by Tikhonov regularization and a completely unreliable distance distribution (Fig. 4d). In contrast, the DEER trace acquired with the HEMT setup provides a well-resolved peak at the expected Cu(II)-Cu(II) distance. The estimated SNR improvement is about 10, which agrees well with the coal measurements at 10 K, despite the complexity of the DEER experiment.

Our probehead enhances the X-band nitroxide DEER sensitivity by a factor of approximately 6-7, which brings it significantly closer to the sensitivity of a high-power Q-band setup, which was estimated previously to be 10-20 times more sensitive than standard commercial X-band setup [33–35]. X-band DEER is also a valuable technique for spin la-

bels that have field-dependent spectral broadening, as is the case for the Cu(II) ruler. Recently, a dedicated comparison of dipolar spectroscopy with Cu(II) metal ions pointed out that sensitivity of Cu(II) DEER is approximately the same at X- and Q-bands due to compensating effects of concentration sensitivity versus spectral width at the two bands [36]. Thus, the observed 10-fold SNR enhancement for Cu(II) X-band DEER represents a significant improvement over the state of the art, which is not expected to be surpassed by using a higher frequency setup.

We expect a similar SNR enhancement for alternative pulsed dipolar spectroscopy techniques such as the relaxation-induced dipolar modulations enhancement (RIDME) [37], the single-frequency technique for dipolar refocusing (SIFTER) [38], and the double quantum coherence (DQC) [39], which can be beneficial depending on the type of sample and spin label. For example, RIDME can outperform DEER for broad metal ion spectra (e.g. Gd(III) [40, 41]), or orthogonal spin lables [42, 43]. X-band RIDME is currently not a common choice for distance measurements, because unwanted signal contributions from nuclear modulation can lead to strong artifacts [36]. Artifact suppression protocols have been developed [42, 44, 45], but strong suppression comes at the cost of sensitivity. Thus, the HEMT setup could provide an important enabler for X-band RIDME in distance measurements with sample concentrations relevant for biological studies.

3.4. Limitations and Further Improvements

The main shortcoming of our probehead is reduced microwave power for spin excitation due to the directional coupler. This prevents measurements of $S = 1/2$ spins using very short π-pulses in the maximally overcoupled resonator. A 6 dB power loss halves the pulse bandwidth, which in some experiments can result in a substantial loss of sensitivity. For example, SNR of our DEER measurements using the ordinary setup could be likely further improved using shorter pulses. However, less overcoupling can be used to compensate for the power loss given the resonator can still accommodate the pulse bandwidth and the prolonged deadtime can be tolerated, the latter always being the case in DEER experiments. Alternatively, one could also use a directional coupler with lower (e.g. 3 dB) coupling value or replace it with a cryogenic circulator, which must be well shielded from the magnetic field. However, either approach would result in less SNR gain, as more room-temperature noise would reach the overcoupled resonator and be reflected to the detection circuit [8]. As a result, there is a trade-off between maximum pulse power and SNR, and optimum values are likely to vary depending on different spin systems under investigation or experiments being performed. At some additional expense, the loss in power could be compensated by using a higher-power TWT amplifier.

Other limitations in the circuit used here arise from the limiter, which has a 200 ns maximum recovery time and 0.1% maximum duty cycle. The recovery time may slightly prolong the deadtime of the spectrometer, although we did

not observe any distortions of the Hahn echo for $\tau = 120$ ns. The duty cycle means that care is required when adjusting the shot repetition time for sequences that consist of very long microwave pulses.

The HEMT is also likely to saturate at lower signal powers compared to the microwave amplifier in the Bruker microwave bridge (the 1 dB compression point of the used HEMT is 0.1 mW). The additional measurements of a very strong echo signal revealed onset of the HEMT saturation (echo clipping). However, measurements of the same echo using a standard setup revealed that such signals almost saturate the digitizer. This demonstrates that the used HEMT has sufficiently wide dynamic range for the majority of samples encountered in EPR.

The SNR enhancement achieved using our setup can be further improved by reducing the losses L_{RH} from the resonator to the HEMT as revealed by Eq. 3 and Fig. 2c. This could be achieved by integrating all microwave components into a single compact three-port device, which would also save highly limited space on the probehead. One could also reduce the losses by removing the microwave switch, although the flat leakage power of the limiter is higher than the maximum input power specified for the preamplifier. Alternatively, the limiter could be removed and a microwave switch capable of handling very high peak powers might be used. However, both cases must be carefully considered to avoid damaging the HEMT, which is the most expensive component in our setup. On the other hand, both components are not necessary for CW experiments as long as the microwave power reaching the preamplifier does not exceed the specified value of 1 mW. Removal of these components is expected to further increase the SNR by a factor of about 1.4.

We used a 30 dB directional coupler to fully suppress the room-temperature noise and obtain the greatest SNR improvement, however, a 15-20 dB coupler should be enough to achieve the same effect while maintaining a relatively high microwave power excitation. Such a setup should allow typical pulsed EPR experiments on high-spin metal centers such as Mn(II) or Gd(III) that require much less microwave power and are important for dipolar spectroscopy [46, 47]. Although less popular in EPR, transmission cavities could permit a simpler receiver design where the directional coupler is replaced by a (physically smaller) attenuator to achieve suppression of room-temperature noise. In principle, room-temperature noise could also be suppressed using orthogonal bimodal transmission cavities [48, 49], which, given sufficient mode isolation, could also remove the need for the attenuator on the input line and the protection circuit in front of the HEMT.

Finally, we note that the probehead design introduced here places the detection circuit at the same temperature as the sample, a key benefit being its compatibility with widely-used cryostats in pulsed EPR. However, new cryostat designs would permit a more versatile arrangement where the HEMT detection circuit is always maintained at cryogenic temperatures (e.g. 4 K), while the sample is in a

variable-temperature environment, potentially remaining at room temperature. This class of cryostat already exists, for example, those with in-built superconducting cryo-magnets and a variable temperature insert (VTI) for the sample - such designs could be further developed to accommodate the microwave receiver circuit at base temperature to offer maximum SNR independently of the sample temperature.

4. Conclusions

We modified and tested a standard X-band EPR probehead by equipping it with an ultra low-noise cryogenic HEMT preamplifier in a circuit that enables usage of high microwave power. Our design does not impact the convenient sample access and resonator coupling found on typical commercial probeheads, and is widely compatible with commercial microwave resonators allowing standard pulsed and CW EPR experiments to be performed as usual while benefitting from significantly improved SNR.

Temperature dependent Hahn echo experiments using the coal standard demonstrated an SNR improvement of almost 8 at 6 K, falling gradually to about 2 at room temperature. This results in a highly significant reduction of the EPR measurement time at low temperatures compared to the standard setup. The full capabilities of the probehead were revealed by performing HYSCORE and DEER experiments on exemplary samples that may be considered challenging for advanced EPR investigations at X-band. In each case, the obtained SNR enhancement was found to be consistent with the Hahn echo experiments of the coal sample.

A further SNR improvement by an additional factor of 2 was obtained by fully suppressing the room-temperature noise on the input line at the expense of reduced pulse power. For experiments that are not excitation-bandwidth limited, this approach shortens the measurement time by a factor of about 200 compared to the standard setup: experiments that would normally take a full day could be performed in less than 10 minutes. Such a gain in sensitivity could be also used to significantly reduce the spin concentration or sample volume allowing studies on systems that are currently not possible at X-band.

Acknowledgement

References

[1] P. Styles, N. Soffe, C. Scott, D. Crag, F. Row, D. White, P. White, A high-resolution NMR probe in which the coil and preamplifier are cooled with liquid helium, J. Magn. Reson. (1969) 60 (1984) 397–404.

[2] P. Styles, N. F. Soffe, C. A. Scott, An improved cryogenically cooled probe for high-resolution NMR, J. Magn. Reson. (1969) 84 (1989) 376–378.

[3] L. Darrasse, J.-C. Ginefri, Perspectives with cryogenic RF probes in biomedical MRI, Biochimie 85 (2003) 915–937.

[4] H. Kovacs, D. Moskau, M. Spraul, Cryogenically cooled probes - a leap in NMR technology, Prog. Nucl. Magn. Reson. Spectrosc. 46 (2005) 131–155.

[5] M. W. Pospieszalski, Extremely low-noise amplification with cryogenic FETs and HFETs: 1970-2004, IEEE Microw. Mag. 6 (2005) 62–75.

[6] W. J. Wallace, R. H. Silsbee, Microstrip resonators for electron-spin resonance, Rev. Sci. Instrum. 62 (1991) 1754–1766.

[7] H. E. Altink, T. Gregorkiewicz, C. A. J. Ammerlaan, Sensitive electron paramagnetic resonance spectrometer for studying defects in semiconductors, Rev. Sci. Instrum. 63 (1992) 5742–5749.

[8] S. Pfenninger, W. Froncisz, J. Hyde, Noise analysis of EPR spectrometers with cryogenic microwave preamplifiers, J. Magn. Reson., Ser. A 113 (1995) 32–39.

[9] G. A. Rinard, R. W. Quine, R. Song, G. R. Eaton, S. S. Eaton, Absolute EPR spin echo and noise intensities, J. Magn. Reson. 140 (1999) 69–83.

[10] J. Zmuidzinas, Superconducting microresonators: physics and applications, Annu. Rev. Condens. Matter Phys. 3 (2012) 169–214.

[11] M. H. Devoret, R. J. Schoelkopf, Superconducting circuits for quantum information: an outlook, Science 339 (2013) 1169–1174.

[12] C. Eichler, A. J. Sigillito, S. A. Lyon, J. R. Petta, Electron spin resonance at the level of 10^4 spins using low impedance superconducting resonators, Phys. Rev. Lett. 118 (2017) 037701.

[13] A. Bienfait, J. J. Pla, Y. Kubo, M. Stern, X. Zhou, C. C. Lo, C. D. Weis, T. Schenkel, M. L. W. Thewalt, D. Vion, D. Esteve, B. Julsgaard, K. Mølmer, J. J. L. Morton, P. Bertet, Reaching the quantum limit of sensitivity in electron spin resonance, Nat. Nanotechnol. 11 (2016) 253–257.

[14] A. Bienfait, P. Campagne-Ibarcq, A. H. Kiilerich, X. Zhou, S. Probst, J. J. Pla, T. Schenkel, D. Vion, D. Esteve, J. J. L. Morton, K. Moelmer, P. Bertet, Magnetic resonance with squeezed microwaves, Phys. Rev. X 7 (2017) 041011.

[15] R. Narkowicz, H. Ogata, E. Reijerse, D. Suter, A cryogenic receiver for EPR, J. Magn. Reson. 237 (2013) 79–84.

[16] Y. Artzi, Y. Twig, A. Blank, Induction-detection electron spin resonance with spin sensitivity of a few tens of spins, Appl. Phys. Lett. 106 (2015) 084104.

[17] S. Probst, A. Bienfait, P. Campagne-Ibarcq, J. J. Pla, B. Albanese, J. F. Da Silva Barbosa, T. Schenkel, D. Vion, D. Esteve, K. Mølmer, J. J. L. Morton, R. Heeres, P. Bertet, Inductive-detection electron-spin resonance spectroscopy with 65 spins/$\sqrt{\text{Hz}}$ sensitivity, Appl. Phys. Lett. 111 (2017) 202604.

[18] G. Grampp, Application of a microwave preamplifier to an ESR spectrometer, Rev. Sci. Instrum. 56 (1985) 2050–2051.

[19] S. Dexheimer, M. Klein, Sensitivity improvement of a Varian E109 EPR spectrometer with a low noise microwave amplifier, Rev. Sci. Instrum. 59 (1988) 764–766.

[20] M. Šimėnas, A. Ciupa, G. Usevicius, K. Aidas, D. Klose, G. Jeschke, M. Maczka, G. Völkel, A. Pöppl, J. Banys, Electron paramagnetic resonance of a copper doped $[(CH_3)_2NH_2][Zn(HCOO)_3]$ hybrid perovskite framework, Phys. Chem. Chem. Phys. 20 (2018) 12097–12105.

[21] N. Le Breton, J. J. Wright, A. J. Y. Jones, E. Salvadori, H. R. Bridges,

J. Hirst, M. M. Roessler, Using hyperfine electron paramagnetic resonance spectroscopy to define the proton-coupled electron transfer reaction at Fe-S cluster N_2 in respiratory complex I, J. Am. Chem. Soc. 139 (2017) 16319–16326.

[22] M. Seif Eddine, F. Biaso, R. Arias-Cartin, E. Pilet, J. Rendon, S. Lyubenova, F. Seduk, B. Guigliarelli, A. Magalon, S. Grimaldi, Probing the menasemiquinone binding mode to nitrate reductase A by selective ^{2}H and ^{15}N labeling, HYSCORE spectroscopy, and DFT modeling, ChemPhysChem 18 (2017) 2704–2714.

[23] J. Rendon, F. Biaso, P. Ceccaldi, R. Toci, F. Seduk, A. Magalon, B. Guigliarelli, S. Grimaldi, Elucidating the structures of the low- and high-pH Mo(V) species in respiratory nitrate reductase: a combined EPR, ^{14,15}N HYSCORE, and DFT study, Inorg. Chem. 56 (2017) 4422–4434.

[24] A. T. Taguchi, P. J. O'Malley, C. A. Wraight, S. A. Dikanov, Determination of the complete spin density distribution in ^{13}C-labeled protein-bound radical intermediates using advanced 2D electron paramagnetic resonance spectroscopy and density functional theory, J. Phys. Chem. B 121 (2017) 10256–10268.

[25] J. Harmer, C. Finazzo, R. Piskorski, C. Bauer, B. Jaun, E. C. Duin, M. Goenrich, R. K. Thauer, S. Van Doorslaer, A. Schweiger, Spin density and coenzyme M coordination geometry of the ox1 form of methyl-coenzyme M reductase: a pulse EPR study, J. Am. Chem. Soc. 127 (2005) 17744–17755.

[26] J. J. Wright, J. G. Fedor, J. Hirst, M. M. Roessler, Using a chimeric respiratory chain and EPR spectroscopy to determine the origin of semiquinone species previously assigned to mitochondrial complex I, BMC Biology 18 (2020) 54.

[27] T. Maly, T. Prisner, Relaxation filtered hyperfine spectroscopy (REFINE), J. Magn. Reson. 170 (2004) 88–96.

[28] A. Silakov, E. J. Reijerse, S. P. J. Albracht, E. C. Hatchikian, W. Lubitz, The electronic structure of the H-cluster in the [FeFe]-hydrogenase from Desulfovibrio desulfuricans: a Q-band ^{57}Fe-ENDOR and HYSCORE study, J. Am. Chem. Soc. 129 (2007) 11447–11458.

[29] I. García-Rubio, M. Fittipaldi, F. Trandafir, S. Van Doorslaer, A multifrequency HYSCORE study of weakly coupled nuclei in frozen solutions of high-spin aquometmyoglobin, Inorg. Chem. 47 (2008) 11294–11304.

[30] L. Liesum, A. Schweiger, Multiple quantum coherence in HYSCORE spectra, J. Chem. Phys. 114 (2001) 9478–9488.

[31] G. Jeschke, DEER distance measurements on proteins, Annu. Rev. Phys. Chem. 63 (2012) 419–446.

[32] G. Jeschke, V. Chechik, P. Ionita, A. Godt, H. Zimmermann, J. Banham, C. R. Timmel, D. Hilger, H. Jung, DeerAnalysis2006 - a comprehensive software package for analyzing pulsed ELDOR data, Appl. Magn. Reson. 30 (2006) 473–498.

[33] E. Bordignon, S. Bleicken, New limits of sensitivity of site-directed spin labeling electron paramagnetic resonance for membrane proteins, Biochim. Biophys. Acta - Biomembranes 1860 (2018) 841–853.

[34] Y. Polyhach, E. Bordignon, R. Tschaggelar, S. Gandra, A. Godt, G. Jeschke, High sensitivity and versatility of the DEER experiment on nitroxide radical pairs at Q-band frequencies, Phys. Chem. Chem. Phys. 14 (2012) 10762–10773.

[35] R. Tschaggelar, F. D. Breitgoff, O. Oberhänsli, M. Qi, A. Godt, G. Jeschke, High-bandwidth Q-band EPR resonators, Appl. Magn. Reson. 48 (2017) 1273–1300.

[36] F. D. Breitgoff, K. Keller, M. Qi, D. Klose, M. Yulikov, A. Godt, G. Jeschke, UWB DEER and RIDME distance measurements in Cu(II)-Cu(II) spin pairs, J. Magn. Reson. 308 (2019) 106560.

[37] S. Milikisyants, F. Scarpelli, M. G. Finiguerra, M. Ubbink, M. Huber, A pulsed EPR method to determine distances between paramagnetic centers with strong spectral anisotropy and radicals: The dead-time free RIDME sequence, J. Magn. Reson. 201 (2009) 48–56.

[38] G. Jeschke, M. Pannier, A. Godt, H. Spiess, Dipolar spectroscopy and spin alignment in electron paramagnetic resonance, Chem. Phys. Lett. 331 (2000) 243–252.

[39] P. P. Borbat, J. H. Freed, Multiple-quantum ESR and distance measurements, Chem. Phys. Lett. 313 (1999) 145–154.

[40] K. Keller, V. Mertens, M. Qi, A. I. Nalepa, A. Godt, A. Savitsky, G. Jeschke, M. Yulikov, Computing distance distributions from dipolar evolution data with overtones: RIDME spectroscopy with Gd(III)-based spin labels, Phys. Chem. Chem. Phys. 19 (2017) 17856–17876.

[41] A. Collauto, V. Frydman, M. D. Lee, E. H. Abdelkader, A. Feintuch, J. D. Swarbrick, B. Graham, G. Otting, D. Goldfarb, RIDME distance measurements using Gd(III) tags with a narrow central transition, Phys. Chem. Chem. Phys. 18 (2016) 19037–19049.

[42] I. Ritsch, H. Hintz, G. Jeschke, A. Godt, M. Yulikov, Improving the accuracy of Cu(II)-nitroxide RIDME in the presence of orientation correlation in water-soluble Cu(II)-nitroxide rulers, Phys. Chem. Chem. Phys. 21 (2019) 9810–9830.

[43] J. L. Wort, K. Ackermann, A. Giannoulis, A. J. Stewart, D. G. Norman, B. E. Bode, Sub-micromolar pulse dipolar EPR spectroscopy reveals increasing Cu^{II}-labelling of double-histidine motifs with lower temperature, Angew. Chem., Int. Ed. 58 (2019) 11681–11685.

[44] D. Abdullin, F. Duthie, A. Meyer, E. S. Müller, G. Hagelueken, O. Schiemann, Comparison of PELDOR and RIDME for distance measurements between nitroxides and low-spin Fe(III) ions, J. Phys. Chem. B 119 (2015) 13534–13542.

[45] I. Ritsch, Distributions of Molecular Conformations and Interactions Revealed by EPR Spectroscopy - Methodology and Application to HnRNPA1, Doctoral Thesis, ETH Zürich (2019).

[46] E. Matalon, T. Huber, G. Hagelueken, B. Graham, V. Frydman, A. Feintuch, G. Otting, D. Goldfarb, Gadolinium(III) spin labels for high-sensitivity distance measurements in transmembrane helices, Angew. Chem., Int. Ed. 52 (2013) 11831–11834.

[47] K. Keller, M. Zalibera, M. Qi, V. Koch, J. Wegner, H. Hintz, A. Godt, G. Jeschke, A. Savitsky, M. Yulikov, EPR characterization of Mn(II) complexes for distance determination with pulsed dipolar spectroscopy, Phys. Chem. Chem. Phys. 18 (2016) 25120–25135.

[48] G. A. Rinard, R. W. Quine, B. T. Ghim, S. S. Eaton, G. R. Eaton, Easily tunable crossed-loop (bimodal) EPR resonator, J. Magn. Reson., Ser. A 122 (1996) 50–57.

[49] G. A. Rinard, R. W. Quine, J. McPeak, L. Buchanan, S. S. Eaton, G. R. Eaton, An X-band crossed-loop EPR resonator, Appl. Magn. Reson. 48 (2017) 1219–1226.